Theor. Appl. Climatol. 89, 155–170 (2007)
DOI 10.1007/s00704-006-0265-1
Printed in The Netherlands

Theoretical and Applied Climatology

State Key Laboratory of Numerical Modeling for Atmospheric Sciences and Geophysical Fluid Dynamics (LASG), Institute of Atmospheric Physics, Chinese Academy of Sciences, Beijing, China

# Interannual variability in the onset of the summer monsoon over the Eastern Bay of Bengal

**J. Mao** and **G. Wu**

With 7 Figures

Received December 8, 2005; revised May 4, 2006; accepted July 12, 2006
Published online October 30, 2006 

**Summary**

Climatological characteristics associated with summer monsoon onset over the eastern Bay of Bengal (BOB) are examined in terms of the westerly-easterly boundary surface (WEB). The vertical tilt of the WEB depends on the horizontal meridional temperature gradient (MTG) near the WEB, under the constraint of the thermal wind balance. The switch in the WEB tilt firstly occurs between 90 and 100°E during the first pentad of May. At this time the 850 hPa ridgeline splits over the BOB and heavy rainfall commences over the eastern BOB, indicating the onset of the BOB summer monsoon (BOBSM). The area-averaged MTG (200–500 hPa) is proposed as an index to define the BOBSM onset. A comparison of the onset determined by the MTG, 850 hPa zonal wind, and outgoing longwave radiation (OLR) shows that the MTG index is the most effective in characterizing the interannual variability of the BOBSM onset.

Strong precursor signals are found prior to an anomalous BOBSM onset. Composite results show that early (late) BOBSM onset follows excessive (deficient) rainfall over the western Pacific and anomalous lower tropospheric cyclonic circulation which extends zonally from the northern Indian Ocean into the western Pacific, and strong (weak) equatorial westerly anomalies in the preceding winter and spring. Prior to an early (late) BOBSM onset, significant positive (negative) thickness anomalies exist around the Tibetan Plateau, accompanied by anomalous upper tropospheric anticyclonic (cyclonic) circulation. The interannual variations of the BOBSM onset are significantly correlated with anomalous sea surface temperature related to ENSO. These occurs through changes in the Walker circulation and local Hadley circulation, leading to middle and upper tropospheric temperature anomalies over the Asian sector. The strong precursor signals around the Tibetan Plateau may be partly caused by local snow cover anomalies, and an early (late) BOBSM onset is preceded by less (more) snow accumulation over the Tibetan Plateau during the preceding winter.

## 1. Introduction

The onset of the summer monsoon is one of the most important sub-seasonal phenomena within the annual cycle. A late or early onset of the monsoon may have devastating effects on agriculture even if the mean annual rainfall is normal. Therefore, forecasting the timing of the onset is critical as it defines ploughing and planting times in agrarian societies in the monsoon regions (Webster et al., 1998).

The monsoon may be thought of as the circulation responding to the annual cycle of solar heating in an interactive ocean–atmosphere–land system (Webster et al., 1998), which is controlled by the thermal contrast between land and ocean. Thus, monsoon onset occurs along with the transition from winter to summer. During monsoon onset some dramatic changes occur in the large-scale atmospheric structure over the monsoon region. Among them is a rapid increase of the

daily rainfall, a change in the low-level wind direction, a sudden establishment of the ''monsoon vortex'' and so on (e.g. Krishnamurti et al., 1981; Krishnamurti, 1985; Chan et al., 2000; Ding and Liu, 2001). Based on these characteristics around monsoon onset, myriad local indices with objective or subjective criteria have been proposed to define the onset dates over different parts in the Asian monsoon region. For example, Ananthakrishnan and Soman (1988) used observational station rainfall with objective criteria to determine the southern Indian monsoon onset dates over Kerala, and Xie et al. (1998) used a combined zonal wind (850 hPa) and outgoing longwave radiation (OLR) index to define the South China Sea (SCS) summer monsoon onset dates for individual years. Based on rain gauge observations and proxy rainfall data derived from satellites, many previous studies have investigated the climatological onset dates of the Asian summer monsoon (e.g. Tao and Chen, 1987; Tanaka, 1992; Lau and Yang, 1997; Webster et al., 1998). However, significant disagreements exist among these studies due to the use of different datasets and different definitions of the onset. Since there are large differences between regional monsoon sub-systems in terms of large-scale circulation, and since the monsoon onset of each sub-system has considerable interannual variability, it is difficult to seek a universal definition for monsoon onset. Therefore, the characteristics associated with monsoon onset should be further explored.

Wu and Zhang (1998) found that in 1989, the Asian summer monsoon onset consisted of three sequential stages. The first occurred over the eastern Bay of Bengal (BOB), the second over the SCS, and the third over South Asia. A similar situation occurred in 1998 (Xu and Chan, 2001). Recently, Wang and LinHo (2002) attempted to build a universal rainfall-based definition for the quantitative description of monsoon climatology for the entire Asian–Pacific domain, and they proposed the relative climatological pentad mean (CPM) rainfall rate as a parameter to define the monsoon onset, peak, and withdrawal of the rainy season. The relative CPM rainfall rate is derived from the difference between the pentad mean and the January mean precipitation rates, thus the monsoon onset date is defined as the pentad when the relative CPM rainfall rate exceeds 5 mm $day^{-1}$. It is shown that the earliest summer monsoon onset occurs over the eastern Bay of Bengal (5–15°N, 90–100°E) around the end of April through early May in the Asian–Pacific monsoon regime (see fig. 1 of Wang and LinHo, 2002). Following this initial stage, the monsoon onset extends northeastward and northwestward. LinHo and Wang (2002) also designed the Asian–Pacific summer monsoon calendar at various key locations, in which the southern Bay of Bengal and southern Burma undergo the earliest onset and the longest rainy season. In an investigation of the relationship between the onset of the Asian summer monsoon and the structure of the Asian subtropical anticyclone, Mao et al. (2004) found that the switch in the tilt of the ridge surface of the subtropical anticyclone belt is closely associated with the Asian monsoon onset. The ridge surface of the subtropical anticyclone is defined by the boundary between the westerly winds to the north and easterly winds to the south [or the westerly-easterly boundary surface (WEB) in brief]. It is obvious that the tilt of the WEB firstly changes from southward to northward between 90 and 100°E during the first pentad of May, with the 850 hPa ridgeline splitting over the Bay of Bengal (BOB), indicating the summer monsoon onset over the eastern BOB (see fig. 3 of Mao et al., 2004). These results suggest that the BOB summer monsoon (BOBSM) onset may be considered as a precursor to the subsequent establishment of the monsoon rainy season. In other words, the study of the BOBSM onset has important significance for understanding Asian monsoon variability.

Geographically, the BOB and the Tibetan Plateau are roughly located along the same longitudinal band. It is intuitively obvious that the Tibetan Plateau should have an important impact on an early/late monsoon onset. The roles played by the Tibetan Plateau in the evolution of the Asian monsoon have been discussed in many studies (e.g. Flohn, 1957; Yanai et al., 1992; Wu and Zhang, 1998). As suggested by Flohn (1957), Li and Yanai (1996) found that the reversal of the meridional temperature gradient (MTG), indicated by the difference of the upper tropospheric (200–500 hPa) temperature between 30 and 5°N, first occurs on the south side of the Tibetan Plateau. They suggested that the onset

of the Asian summer monsoon is concurrent with the reversal of the MTG in the upper troposphere. However, as shown by Wang and LinHo (2002), the Asian summer monsoon is not established simultaneously over different parts of Asia. So, the question is, in which latitudinal extent and layers is the MTG capable of indicating monsoon onset for a particular region? Mao et al. (2004) carried out preliminary analyses of the relationship between the MTG and the WEB, and how the MTG determines the SCS summer monsoon onset. The potential applications of the MTG in measuring the monsoon onset over the BOB and other regions deserve further study.

It is well known that the Asian monsoon is significantly linked with ENSO (e.g. Meehl, 1987; Ju and Slingo, 1995; Kawamura, 1998; Zhang et al., 2002). Webster and Yang (1992) studied the interannual variability of the broad-scale Asian summer monsoon and identified strong signals in monsoon variability in the upper tropospheric westerlies over subtropical Asia during the winter and spring seasons, and also suggested that the monsoon and ENSO are selectively interactive systems. Joseph et al. (1994) found that most delayed southern Indian monsoon onsets are associated with warm sea surface temperature (SST) anomalies at, and south of, the equator in the Indian and Pacific Oceans, and cold SST anomalies in the tropical and subtropical oceans to the north during the season prior to the monsoon onset. This indicates that ENSO is one of the important factors influencing the interannual variability of the Asian monsoon onset. Some studies show that snow cover, as an external forcing, can influence the interannual variability of the atmospheric circulation due to changes in the surface energy balance and land surface hydrological processes (e.g. Walsh et al., 1985; Barnett et al., 1989; Yang and Lau, 1996). Hahn and Shukla (1976) found that Indian summer monsoon rainfall is negatively related to Eurasian snow cover in the preceding spring. Dey and Kathuria (1986) showed the southern Indian monsoon onset is also associated with the Himalayan snow cover area. Heavy snowfall during winter leads to a weakened summer monsoon circulation caused by the weak heat contrast between the Eurasian continent and the Indian Ocean (Yasunari et al., 1991). Based on the observational snow depth dataset over the Tibetan Plateau, Wu and Qian (2003) re-examined the relationship between the Tibet winter snow anomaly and the subsequent summer rainfall over the Asian monsoon region. How and to what extent the BOBSM onset is significantly linked with these forcings on interannual timescales needs to be answered.

In view of the priority of the BOBSM onset in the Asian monsoon regime, the objectives of this paper are to identify the BOBSM onset date based on the MTG and to examine the factors during the preceding winter and spring that influence the interannual variability of the BOBSM onset. The slowly varying boundary conditions such as SST and snow cover associated with an anomalous monsoon onset are investigated in terms of the contributions to the land–sea thermal contrast.

Section 2 describes the data used in this study. Some characteristics of an abnormal BOBSM are examined in Sect. 3. The precursory signals during the preceding winter and spring and factors that significantly influence the interannual variability of the BOBSM onset are investigated in Sect. 4. Summary and discussion are given in Sect. 5.

## 2. Data

The primary data are global monthly and daily means from the National Centers for Environmental Prediction–National Center for Atmospheric Research (NCEP–NCAR) reanalysis products (Kalnay et al., 1996), which include wind, geopotential height, temperature, vertical velocity, and relative humidity at 17 standard pressure levels, with a horizontal resolution of $2.5 \times 2.5^{\circ}$ from 1958 to 2001. The daily mean climatology is based on the period 1968–1996. These data are obtained directly from the website of the National Oceanic and Atmospheric Administration–Cooperative Institute for Research in Environmental Sciences (NOAA–CIRES) Climate Diagnostics Center.

The Climate Prediction Center (CPC) Merged Analysis of Precipitation (CMAP; Xie and Arkin, 1997) from 1979 to 2001 is derived from the merging of rain gauge observations, five different satellite estimates, and numerical-model outputs. It is used to describe the monsoon rainfall over the entire Asian land and oceans. Since the

CMAP dataset merges multi-source estimates, the uncertainties contained in each individual estimate are significantly reduced. CMAP is available in pentads, at a resolution of $2.5 \times 2.5°$. Daily OLR from NOAA, spanning from June 1974 to December 2001 (except for eight months in 1978), is also a commonly used proxy of tropical convective activity.

Monthly SST for the period 1958–2001 from NOAA extended reconstructed SST datasets are used to investigate the impacts of ENSO on the interannual variability of the BOBSM onset. Also used is the monthly snow depth (SD) over the Tibetan Plateau from 60 stations for the period 1960–1998. The SD is used to quantitatively examine the influences of the Tibetan Plateau snow cover on the atmospheric thickness and wind fields.

## 3. Characteristics of the anomalous BOB monsoon onset

### *3.1 Relationship between the switch of the WEB tilt and the BOBSM onset*

Mao et al. (2004) utilized the WEB to understand the Asian summer monsoon onset. Because the summer monsoon onset occurs as a transition from a cold–dry to a warm–moist season, along with the lower tropospheric wind reversal, it is inevitably related to the changes in temperature, pressure, and wind fields in the entire troposphere through geostrophic and hydrostatic balance constraints. The subtropical anticyclone is a key system that connects the tropical and midlatitude atmospheric circulations, with its ridgeline representing the maximum in geopotential height (Li and Chou, 1998). Since the WEB is also the vertical shear zone between easterlies and westerlies, it represents the three-dimensional structure of the subtropical anticyclone. The WEB can thus be used as a proxy for the essential features of both the pressure and wind fields (Mao et al., 2004). On the other hand, the thermal wind balance suggests that the tilt of the WEB depends on the horizontal MTG in the vicinity of the WEB. Therefore, the WEB always tilts vertically towards the warmer region when the geostrophic relation is valid.

Using climatological pentad mean datasets, Mao et al. (2004) surveyed in detail the switch of the WEB tilt and its association with the Asian summer monsoon onset during the transitional season (see their fig. 3). It is shown that the ''seasonal transition axis'' (STA) first establishes over the eastern BOB and Indochina Peninsula during the first pentad of May. The STA represents a critical state at which the ridge axis in the troposphere is ''vertical'', and can be identified by the crossing points between the 500 and 200 hPa ridgelines. When the WEB tilts northward over eastern BOB and Indochina Peninsula from the second pentad of May, deep convection develops, which represents the onset of the Asian summer monsoon. This change of the WEB tilt indicates a switch from the winter to the summer monsoon. When the tilt of the WEB changes from southward to northward, the MTG in the vicinity of the WEB changes from negative to positive. The MTG is thus a good indicator for identifying the onset of BOBSM.

It should be mentioned that, in practice, the STA is not a convenient index to use to define onset, but it can be highlighted as the critical state at which the MTG is equal to zero. Furthermore, the location of the STA helps to determine a domain to define the onset based on the MTG.

### *3.2 Identifying the onset date based on the MTG*

Seasonal variations in rainfall, 850 hPa winds, and MTG over the eastern BOB are shown in Fig. 1. Heavy precipitation exceeding 6 mm day$^{-1}$ is found over the equatorial region throughout most of the year (Fig. 1a). From the end of April to early May, the rapid northward extension of the heavy rainbelt takes place from 5 to 15°N, accompanied by the commencement of the southwesterlies at low levels (Fig. 1b), indicating a BOBSM onset. Subsequently, the strong southwesterlies are maintained until the end of September. Note also that the reversal of the zonal wind direction is primarily confined to the latitudinal band 5–15°N, and such a reversal is distinct around early May, suggesting that the 850 hPa zonal winds can reflect the BOBSM onset. Moreover, the mean position of the WEB is located within this latitudinal band (see fig. 3 of Mao et al., 2004). Considering these features along with the results shown by Wang and LinHo (2002), we chose the eastern BOB domain (5–15°N, 90–100°E) in this study. When 850 hPa

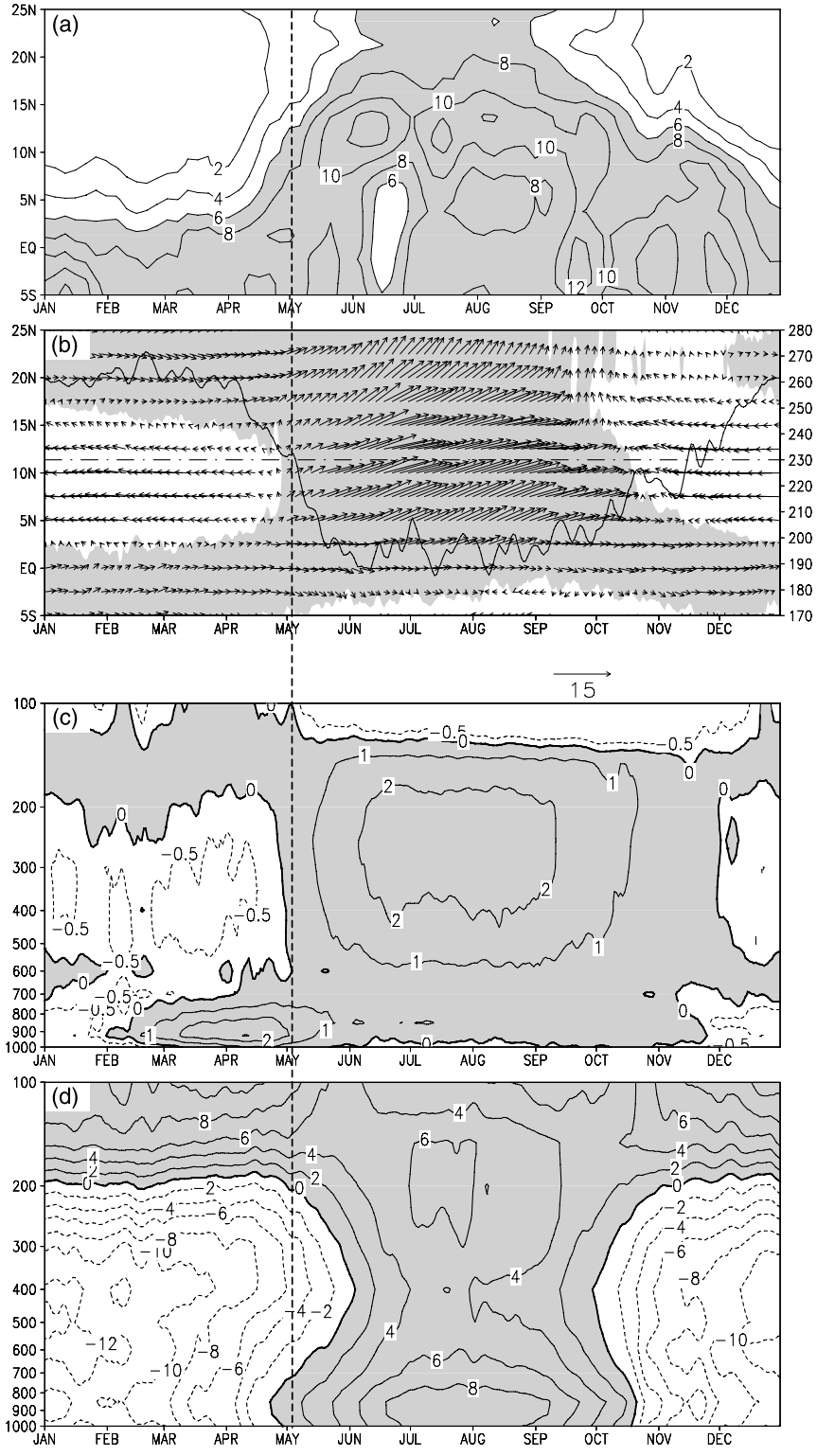


**Fig. 1.** Seasonal evolutions of rainfall, 850 hPa winds, and atmospheric meridional temperature gradient over the eastern BOB (5–15°N, 90–100°E). (**a**) Latitude-time cross section (90–100°E) of the climatological pentad mean Merged Analysis Precipitation from the Climate Prediction Center (mm day$^{-1}$), with shading indicating the precipitation rate exceeding 6 mm day$^{-1}$; (**b**) Latitude-time cross section (90–100°E) of the daily mean 850 hPa winds (m s$^{-1}$), with shading denoting the zonal wind greater than zero. Thick solid line denotes the time series of the area-averaged daily mean OLR (W m$^{-2}$) over the eastern BOB; (**c**) Pressure-time cross section of the area-averaged daily mean meridional temperature gradient ($10^{-6}$ K km$^{-1}$) over the eastern BOB; (**d**) Pressure-time cross section of the meridional temperature gradient ($10^{-6}$ K km$^{-1}$) indicated by the difference between 30 and 5°N and averaged between 90 and 100°E. The shading in (c) and (d) denotes the meridional temperature gradient greater than zero

winds change from easterlies to westerlies, the OLR value rapidly drops to near or below the critical value of 230 W m$^{-2}$ (Fig. 1b).

According to Wang and LinHo (2002), the BOB is a unique region where the South Asian monsoon links with the East Asian monsoon. The former is a typical tropical monsoon system, whereas the latter is a combined tropical-mid-latitude system (Chen and Chang, 1980). The properties of the lower tropospheric southwester-

lies over the BOB during monsoon onset are thus more complex. As suggested by Zhang et al. (2002), there are at least three different branches that contribute to the circulation over the BOB and Indochina Peninsula, in which the southwesterlies leading to BOBSM onset consist of the subtropical westerlies from the Arabian anticyclone and tropical westerlies from the Somali cross-equatorial flow. Therefore, one may question whether the 850 hPa zonal wind index can be constructed to describe the BOB circulation change before, during, and after the monsoon onset. Use of the MTG as an index can avoid this uncertainty. It can be seen that an abrupt reversal of the sign in the MTG occurs in the middle and upper troposphere between 200 and 600 hPa around 2 May (Fig. 1c), which corresponds to the time of the establishment of the STA over the eastern BOB. Note that the reversal of the MTG in the lower layer (700–1000 hPa) is much earlier than in the upper layers, which may be caused by stronger sensible heating over Burma. Although Li and Yanai (1996) pointed out the significance of the MTG (200–500 hPa) to the Asian summer monsoon onset, the mean reversal time, using their calculation – temperature difference between 30 and 5°N, is around the end of May (Fig. 1d). This date is nearly one month later than those shown in Fig. 1a to c, suggesting that the upper tropospheric temperature difference between 30 and 5°N is not suitable as an index for defining the BOBSM onset. The above discussion indicates that in determining the monsoon onset date, the use of the MTG reversal in the vicinity of the WEB is more appropriate since the onset of the low-level monsoon southwesterlies occurs almost simultaneously with the switch of the WEB tilt in the upper troposphere or a break of the lower tropospheric ridgelines.

It is obvious that the BOBSM onset dates (first pentad of May or 2 May), as determined by the above four meteorological quantities (Fig. 1a to c), are fairly consistent, and are also accordant with the results presented by Wang and LinHo (2002). These four elements from several different aspects reflect the main climatological characteristics of the BOBSM onset. Because the wind patterns and origins over the BOB are very complicated as stated above, and the longer daily CMAP and OLR records are unavailable, in this paper we use the area-averaged upper tropospheric (200–500 hPa) MTG over the eastern BOB as a primary index to identify the BOBSM onset date.

Following Mao et al. (2004), the onset date for each individual year is defined as the day when the following criteria are first satisfied: (1) the area-averaged upper tropospheric (200–500 hPa) MTG over the eastern BOB (5–15°N, 90–100°E) changes from negative to positive; (2) the MTG remains positive for more than 10 days. The duration threshold is now selected as 10 days to assure that a true change in the large-scale circulation has occurred because the

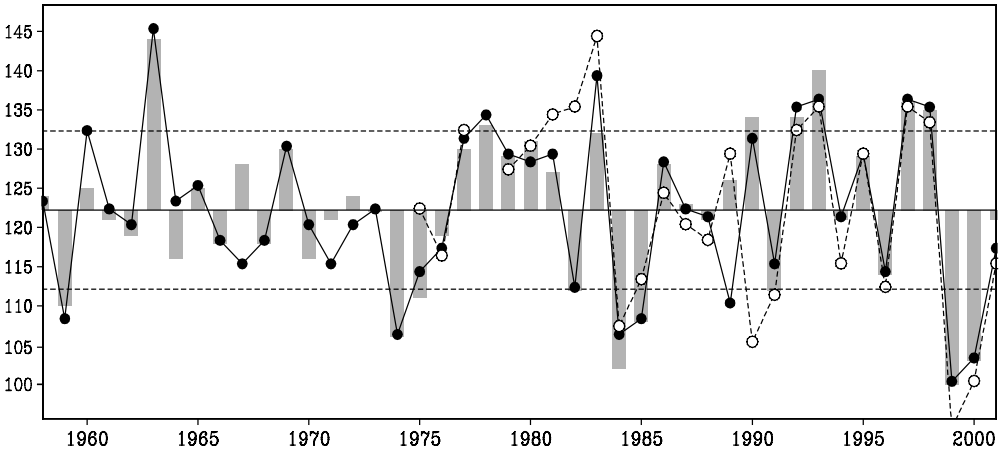


**Fig. 2.** Time series of the BOBSM onset dates defined by the MTG (bars), 850 hPa zonal wind (solid circles), and OLR (open circles) for the period 1958–2001. All dates are Julian dates in the calendar year (e.g. day 121 = 1 May, etc.). The long-term mean onset date for each of three time series is indicated by a solid line. One standard deviation of the time series derived from the MTG index is indicated by the two dashed lines

period of synoptic-scale disturbances is about one week based on previous studies (e.g. Chan et al., 2000). For a comparison, an identical definition is applied to the 850 hPa zonal wind (U850) and OLR, with the threshold of OLR chosen as 230 W $m^{-2}$.

The BOBSM onset dates for each individual year, based on the above definition, are displayed in Fig. 2. It is found that in the majority of years, the dates determined by these three indices are very similar, but there are large differences in a few cases, e.g. in 1967, 1982, 1989, 1990. In these inconsistent years, the occurrence of convection was usually later than the reversals of the MTG and U850. This inconsistency needs to be further examined. These three onset time series are well correlated with each other, exceeding the 99% confidence level. The correlation coefficients of MTG with U850 and with OLR are 0.919 and 0.807, respectively, and the correlation coefficient between U850 and OLR is 0.797. In contrast, the MTG exhibits a better correlation with U850 than with OLR. These indicate that the MTG index is more effective in characterizing the interannual variation of the BOBSM onset.

### *3.3 Interannual variability of the BOBSM onset*

The long-term mean onset dates determined by the MTG, U850 and OLR are 2 May, 2 May, and 1 May, with standard deviations of 10.2, 10.2, and 12.2 days, respectively (Fig. 2). The BOBSM onset dates differ significantly from one year to another, with the range between the earliest and the latest onset dates exceeding one month. Now we examine the interannual variability of the BOBSM onset on the basis of the time series of onset dates derived from the MTG index.

Using one standard deviation as the threshold, we classify an early (late) BOBSM onset as one with its anomaly less (greater) than one standard deviation. Thus, the early onset years selected are 1959, 1974, 1975, 1982, 1984, 1985, 1991, 1999, 2000, while the late onset years are 1963, 1978, 1983, 1990, 1992, 1993, 1997, 1998. Since the abnormal early and late BOBSM onset years are classified, the precursory signals appearing in the preceding winter and spring can be examined in terms of the atmospheric circulation, SST, etc.

## 4. Precursory signals associated with the interannual variability of the BOBSM onset

### *4.1 Atmospheric circulation anomalies*

To examine the remote influences on the interannual variability of the BOBSM onset during the preceding winter and spring, composite analyses were made for early and late onset categories. Composite differences in the 850 hPa winds and precipitation for late winter to spring between early and late onset categories show that an anomalous cyclone is present over the BOB, SCS, and western Pacific, with significant westerlies prevailing in the equatorial region and easterlies in the northwestern BOB (Fig. 3a). Significant easterly anomalies exist over the equatorial central-eastern Pacific. Strong southerly anomalies are also found over the east of the Philippine Sea, due to the convergence between the anomalous equatorial westerlies and easterlies. As a result, positive rainfall anomalies occur in the vicinity of the Philippines (Fig. 3d). The entire flow pattern together with anomalous rainfall is similar to the analytical solution given by Gill (1980). The cyclonic circulation around the Philippines, accompanied by enhanced precipitation, becomes more intense in March, when the equatorial westerlies south of the BOB strengthen and extend northward (Fig. 3b and e). The twin-cyclone or double-low structure suggested by Chen and Chen (1993) in the Indian Ocean appears in April, in which the cyclone to north of the equator is centered over the west coast of the BOB so that the eastern BOB is dominated by significant southwesterlies (Fig. 3c). Importantly, the equatorial westerlies between these two cyclones are strengthened and extend further northward, leading to more moisture transport from the tropical Indian Ocean to the eastern BOB at low levels. Heavy rainfall thus occurs over the eastern BOB and western Indochina Peninsula (Fig. 3f), implying that the BOBSM bursts earlier than normal. The strengthening of the BOB cyclonic circulation and the equatorial westerlies may be attributed to a Rossby wave response to the enhanced convection over the SCS and western Pacific (Gill, 1980), since the significant rainfall domain continuously extends westward from the western Pacific to the Indian Ocean. The westward extension of the significant rainfall

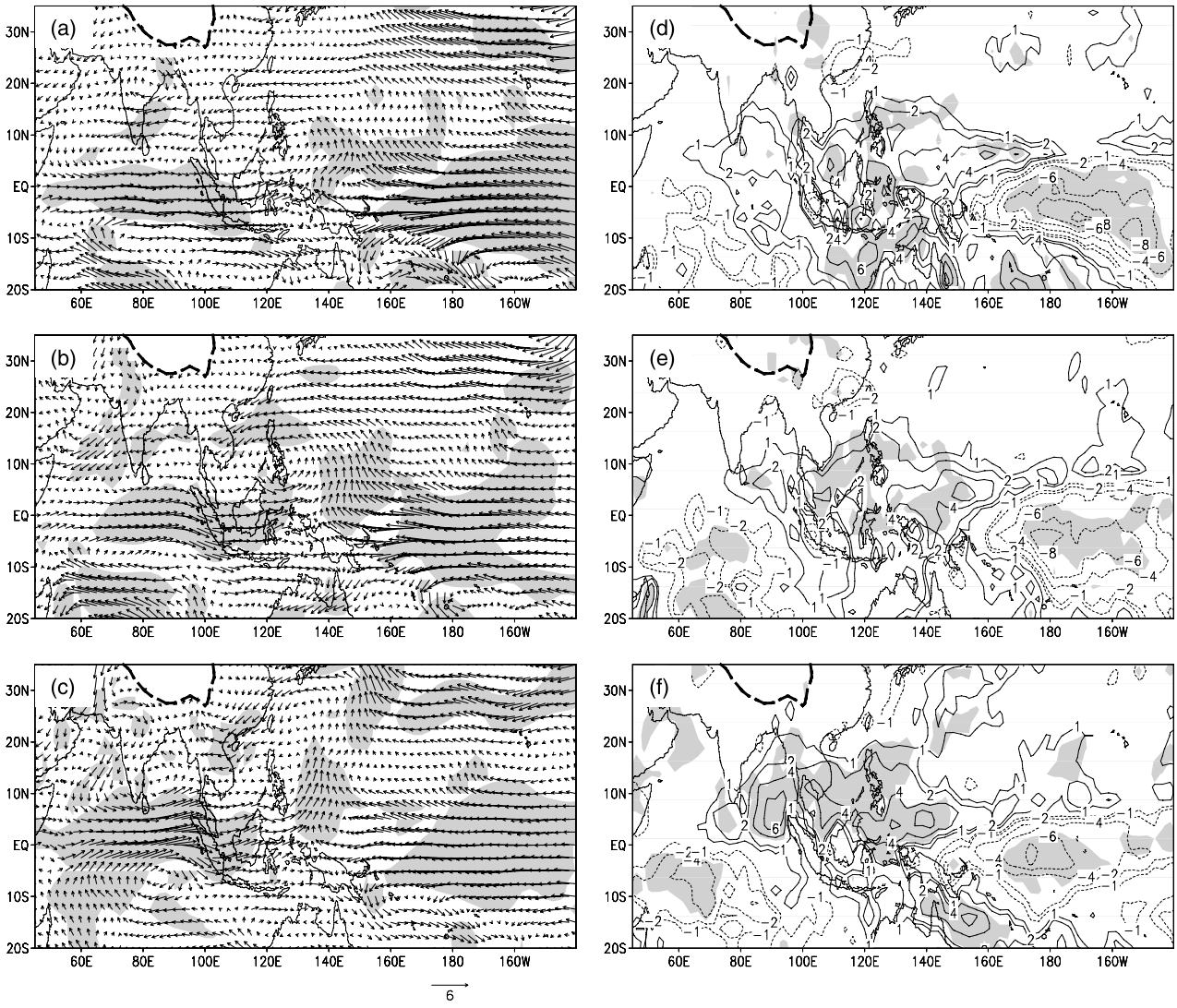


**Fig. 3.** The monthly early-minus-late composite patterns of the differences in 850 hPa wind field from (**a**) to (**c**) and CMAP rainfall from (**d**) to (**f**) for February to April in the preceding late winter and spring. Shading indicates that the *t*-test passes the 95% significance level. In the left panel, shading denotes that at least one of the wind components (zonal or meridional) passes the 95% significance level. Thick dashed line shows the Tibetan Plateau above 3000 m

anomalies around the equator demonstrates a westward Rossby wave propagation.

Composite patterns of the 200 hPa wind differences illustrate that prior to the BOBSM onset, an anomalous anticyclone exists over the vicinity of the Tibetan Plateau for the early onset category. The center of the anticyclone is located over the east of the Tibetan Plateau in February, then moves southwestward so that anomalous easterlies prevail over the northern Indian Ocean from 5°S to 25°N (figures not shown), implying that the upper tropospheric westerly jet south of the Tibetan Plateau is weaker in the winter and spring seasons. In summary, an early (late) BOBSM onset follows excessive (deficient) rainfall over the western Pacific, an anomalous lower tropospheric cyclone (anticyclone) extending from the northern Indian Ocean to the western Pacific, strong (weak) equatorial westerly anomalies, and an anomalous upper tropospheric anticyclone (cyclone) around the Tibetan Plateau with easterly (westerly) anomalies in the preceding winter and spring.

Due to the variation of the subtropical anticyclone being closely related to the Asian monsoon onset, the differences in atmospheric circulation between early and late BOBSM onset should be reflected by the WEB. Composite patterns of the

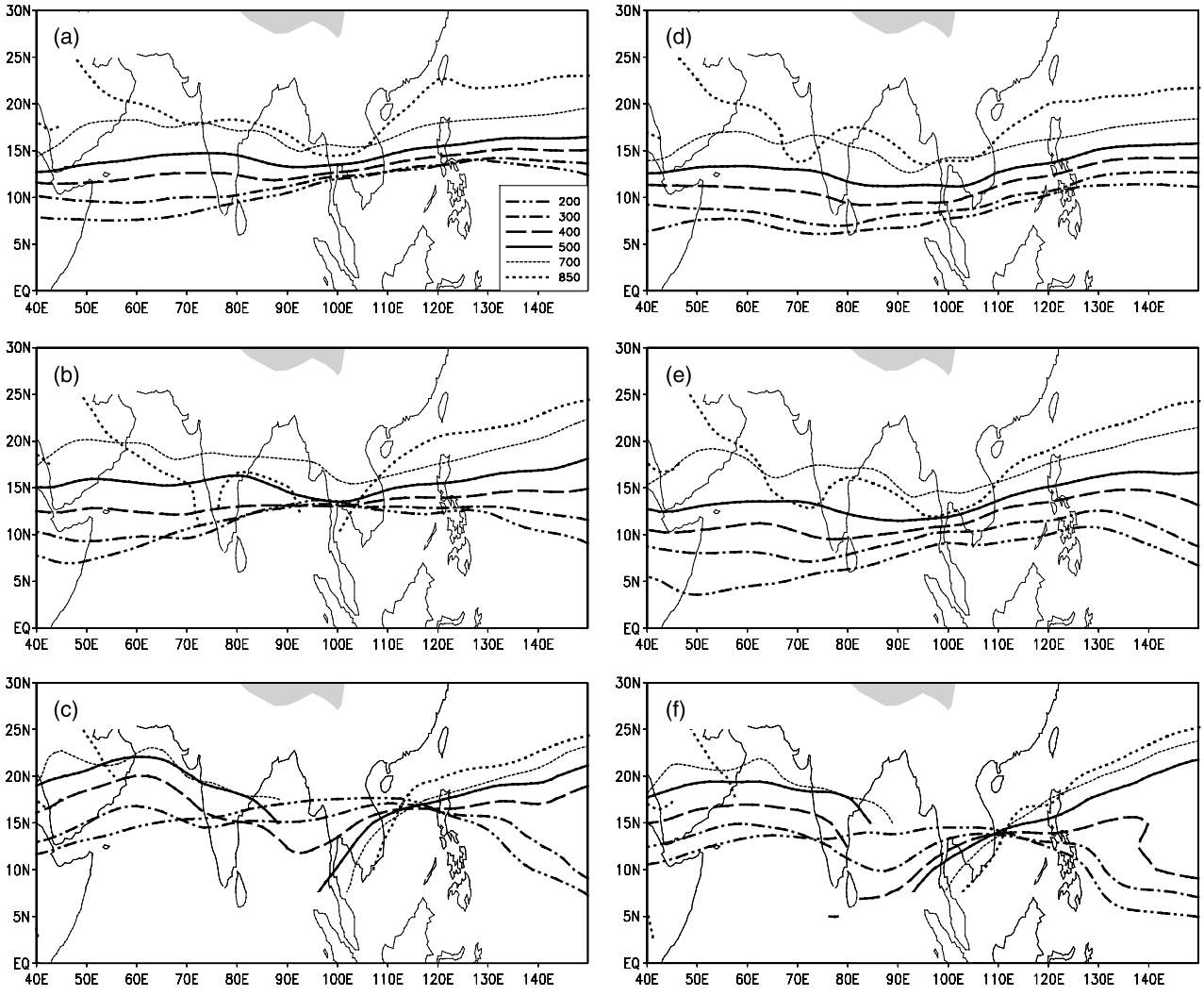


**Fig. 4.** Composite projections of the WEB for early (left panel) and late (right panel) BOBSM onset categories. Projections for March to May are displayed from (**a**) to (**c**) and from (**d**) to (**f**) respectively. Thick curves denote the subtropical anticyclone ridgelines on various isobaric surfaces (indicated by the numbers in legend). Shading denotes terrain above 3000 m

WEB for early and late onset are presented in Fig. 4. Remarkable differences are found within the BOB and Indochina Peninsula longitudes. In March, the ridgelines of the early onset category are closer between 90 and 100°E than those of the late onset category, indicating that the southward tilt of the WEB or the MTG in the region in early onset years is usually weaker than in late onset years (Fig. 4a and d). By April, the WEB above 500 hPa of the early onset category becomes vertical between 90 and 100°E, while the WEB of the late onset category still exhibits a significant southward tilt (Fig. 4b and e). In May, although the WEB tilt in both categories exhibits a northward tilt over the BOB and Indochina Peninsula, some substantial differences exist in the tilt extent and the location of the STA (Fig. 4c and f). Here, the STA can be identified by the crossing point stacked up with the ridgelines at most levels. In the early category, the 200 and 300 hPa ridgelines are located to the north of 15°N, while the STA is situated over the northeastern SCS. Consistently, the upper tropospheric anticyclone is located further north than normal (see also Fig. 2 of Mao et al., 2004), with the lower tropospheric southwesterlies prevailing in broader longitudes. For the late category, the STA is only located at the western coast of the SCS, and the northward tilt of the WEB is smaller.

### *4.2 Temperature and thickness anomalies*

Lagged correlations between the BOBSM onset date and the upper tropospheric (200–500 hPa) thickness for January to April show that significantly positive correlation areas appear over the eastern Pacific, indicating remote influences of the Pacific Ocean on the BOBSM onset (not shown). Pronounced positive correlation areas exist over Lake Baikal in February and March. It is stressed here that the negative correlation is particularly strong around the Tibetan Plateau. A small negative correlation area is observed over East China in January, then becomes larger and stronger, and moves steadily westward, forming a large significant negative area over the Tibetan Plateau. Such a significant correlation area reflects the thermal effect of the Tibetan Plateau. That is, the thermal anomaly of the Tibetan Plateau in the winter and spring may have an important impact on the temperature anomalies to the north side of the WEB, leading to the change of the land–sea thermal contrast across the WEB.

To examine the detailed features over the Tibetan Plateau, composite patterns of upper tropospheric (200–500 hPa) thickness and 600 hPa temperature differences between the early and late BOBSM onset categories are shown in Fig. 5. Corresponding to the correlation pattern, an area of significantly positive thickness anomalies is observed over central China in February (Fig. 5a), and then extends westward, with its

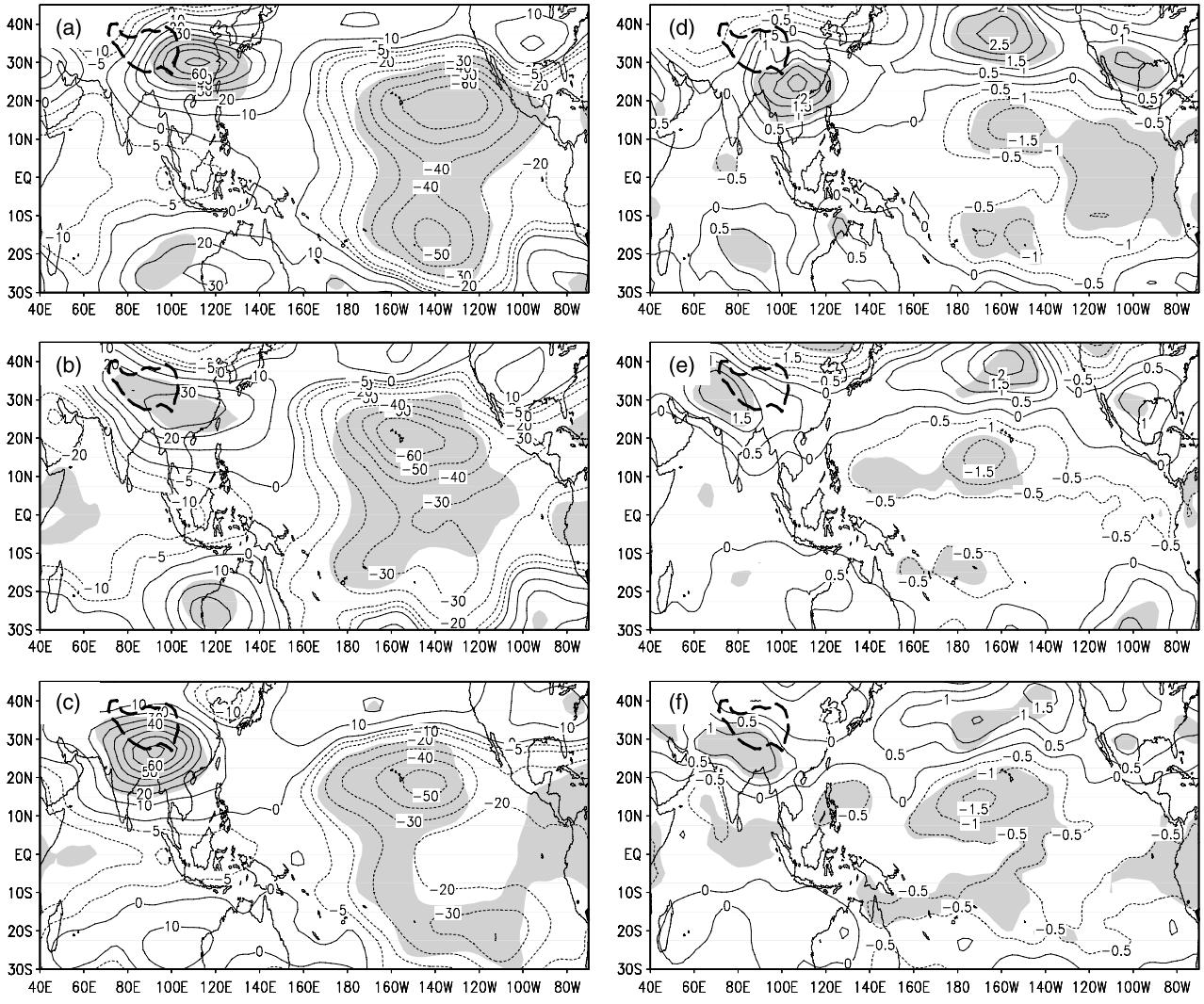


**Fig. 5.** The monthly early-minus-late composite patterns of the differences in the upper tropospheric (200–500 hPa) thickness from (**a**) to (**c**) and 600 hPa air temperature from (**d**) to (**f**) for February to April in the preceding late winter and spring. Shading indicates that the *t*-test passes the 95% significance level. Thick dashed line shows the Tibetan Plateau above 3000 m

center just over the southeastern Tibetan Plateau (Fig. 5b), forming an anomalously strong meridional contrast of thickness characterized by positive anomalies over the Tibetan Plateau north of 15°N, and negative anomalies over the tropical Indian Ocean. In April (Fig. 5c), the thickness anomaly area is centered on the south side of the Tibetan Plateau (along 90°E), resulting in a pattern similar to that shown in Li and Yanai (1996). The Tibetan Plateau surface is close to the 600 hPa isobaric surface, and so the 600 hPa temperature anomalies are chosen to highlight the thermal effects of the Tibetan Plateau (Fig. 5d to f). Similar to upper tropospheric thickness anomalies, significant differences in 600 hPa temperature are found over the Tibetan Plateau and Indian Ocean, paticularly in April, indicating a contribution to the thermal contrast between land and ocean in the middle troposphere. Early (late) BOBSM onset is preceded by positive (negative) temperature anomalies over the Tibetan Plateau in the middle and upper troposphere. Notice that significant thickness anomalies with a butterfly pattern exist over the Pacific sector, which indicates the atmospheric response to ENSO heating over the equatorial eastern Pacific region. Such a thickness anomaly pattern may be associated with the temperature anomalies over the Tibetan Plateau (Miyakoda et al., 2003).

Our correlation and composite patterns are similar to those discussed by Miyakoda et al. (2003), who investigated pre-monsoon signals of the South Asian monsoon over the Tibetan Plateau and their association with ENSO (see their figs. 1 and 2). They defined an index that is also called MTG, indicating the Asian summer monsoon intensity, and they calculated the lagged correlation between this index and the upper tropospheric (200–500 hPa) thickness for different seasons. As in Miyakoda et al. (2003), in addition to the high correlation over the equatorial region, the westward migration of high correlation around the Tibetan Plateau is very significant from winter to summer. These results suggest that the upper tropospheric temperature anomaly over the Tibetan Plateau can foreshow

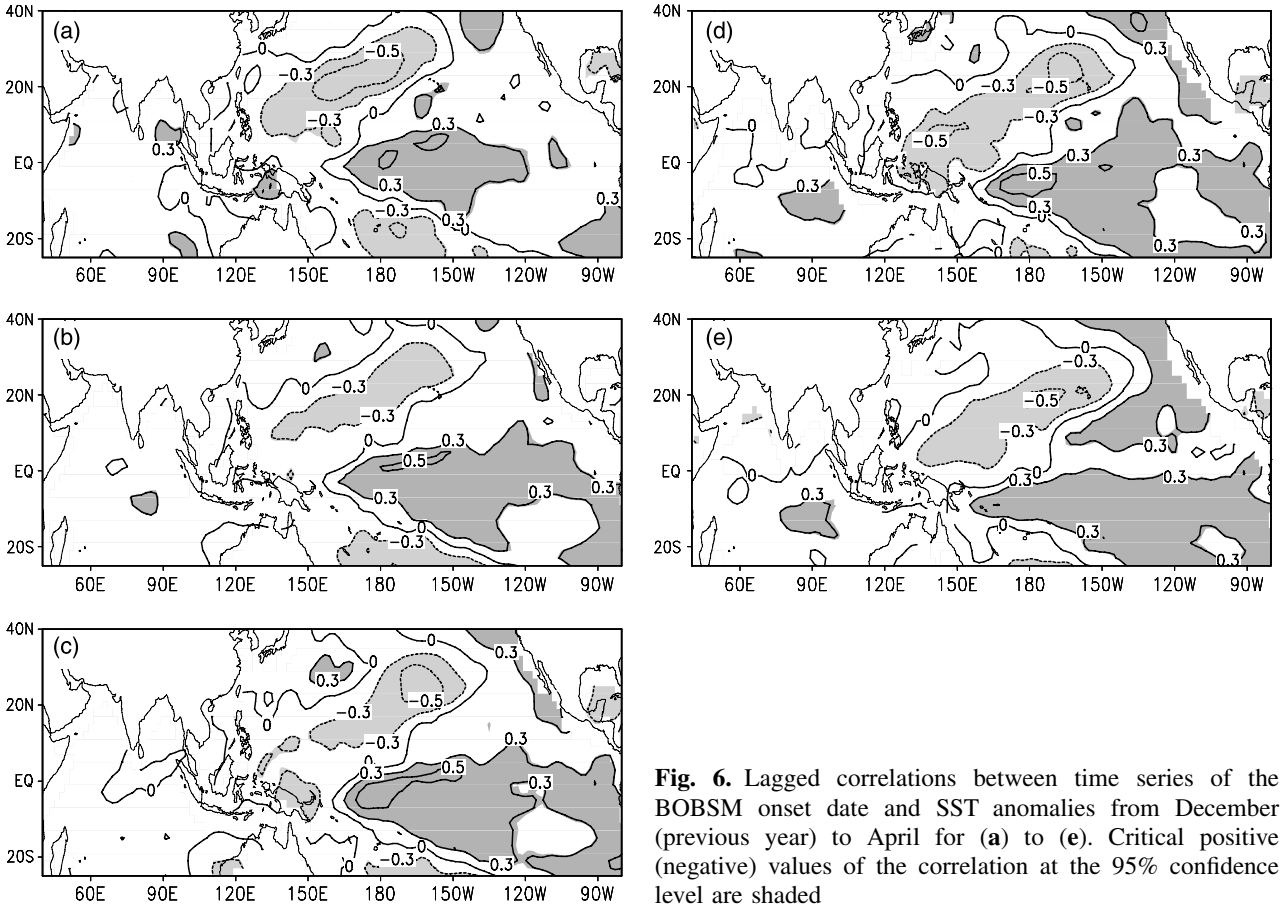


**Fig. 6.** Lagged correlations between time series of the BOBSM onset date and SST anomalies from December (previous year) to April for (**a**) to (**e**). Critical positive (negative) values of the correlation at the 95% confidence level are shaded

not only the South Asian summer monsoon intensity but also the BOBSM onset, and it may provide a precursory background for anomalous BOBSM onset and anomalous intensity of the South Asian summer monsoon.

### *4.3 SST and Snow anomalies*

Since atmospheric anomalies cannot persist for several months without any external forcing, the aforementioned persistent signals associated with abnormal BOBSM onset are difficult to explain by atmospheric processes alone. As suggested by Miyakoda et al. (2003), the presence of these precursory signals may be related to anomalous SST forcing. We thus investigate remote influences involving snow cover and SST.

Figure 6 shows lagged correlations between the BOBSM onset date and SST during the preceding winter and spring. Significant positive correlations are observed over the equatorial central and eastern Pacific, with negative correlations extending from the equatorial western Pacific to the North Pacific of middle latitude. Positive correlations are also found over the equatorial Indian Ocean from March to May, reflecting that the SST anomalies over the Indian Ocean are usually later than those over the equatorial Pacific during an ENSO event (Trenberth, 1990; Sewell and Landman, 2001). The entire pattern of correlations strongly resembles the SST anomaly in an El Niño event from December to April. To further validate the relationship between ENSO and the abnormal BOBSM onset, we also calculate the correlation coefficient between the normalized time series of the BOBSM onset date and Niño 3.4 SST index for the period 1958–2001. The correlation coefficient of the BOBSM onset date with Niño 3.4 SST index for February is 0.44, exceeding the 99% confidence level. The BOBSM-ENSO relationship seems to have undergone a decadal change. Prior to 1967 the magnitude of the onset date anomalies was weak and its correlation with eastern Pacific SST anomalies was weakly negative. Since 1968 the correlation has been stronger, with a correlation coefficient value of 0.58 for the period 1968–2001. In fact, the correlation coefficient of the BOBSM onset date with the Niño 4 SST index is higher than with the Niño 3.4 SST index for December to March. The above suggests that an El Niño (La Niña) event is followed by late (early) BOBSM onset.

Zhang et al. (2002) found that the interannual variation of the Asian summer monsoon onset over the Indochina Peninsula is closely related to El Niño/La Niña during the boreal spring. They suggested that the changes in the Walker circulation and the local Hadley circulation, as a direct response to ENSO, lead to anomalous convective activities over the equatorial Pacific. Similar situations can be seen from Fig. 3. From February to April, significantly positive rainfall anomalies over the western Pacific are concurrent with westerly anomalies over the Indian Ocean-western Pacific, while negative rainfall anomalies correspond to easterly anomalies over the central-eastern Pacific. These suggest that the changes of the Walker circulation and the local Hadley circulation forced by ENSO may be responsible for an early/late BOBSM onset.

Namias et al. (1988) pointed out that persistent SST anomalies in the North Pacific are usually associated with the atmospheric teleconnection patterns. The impact of ENSO on the BOBSM onset can be further understood by the study of Miyakoda et al. (2003), which suggested that the air temperature anomaly between 200 and 500 hPa and its westward movement over the Asian sector along 20–35°N are associated with the butterfly pattern over the Pacific sector. In our study, composite patterns of thickness anomalies (Fig. 5) are similar to the result from Miyakoda et al. (2003) for strong and weak monsoons (see their fig. 8). The butterfly pattern over the Pacific sector is essentially a Gill-type response to the tropical heat source (Gill, 1980). Corresponding to the butterfly pattern, the symmetrical circulations associated with Hadley Cells are thus produced in both hemispheres when positive heat sources of a short longitudinal length appear at the equator. Such a flow pattern has been verified by some numerical simulations (e.g. Ting and Held, 1990). Wu and Newell (1998) used the Gill-type model to examine the tropical atmospheric response to an El Niño event. A local heat source can warm the entire tropical troposphere when the heat source appears in the equatorial eastern Pacific. The released latent heat and its forced adiabatic subsidence elsewhere in the Tropics can warm the atmosphere. The tropospheric atmosphere thus becomes warm over the

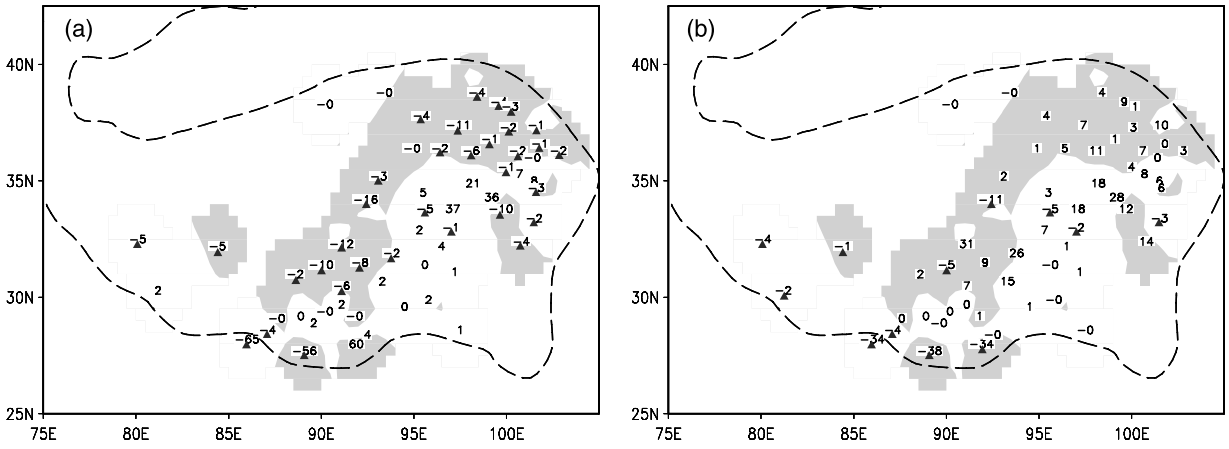


**Fig. 7.** Composite distributions of Nov.–Mar. accumulated snow depth anomalies (cm month$^{-1}$) over the Tibetan Plateau for (**a**) early and (**b**) late BOBSM onset categories. Negative anomalies are marked with triangles. Shading denotes the regions where the *t*-test is significant at 90% confidence level. Dashed line shows the Tibetan Plateau above 2500 m

equatorial Indian Ocean, affecting the land–sea thermal contrast over the Asian sector.

In addition to the association with the teleconnection forced by ENSO, the signals over the Tibetan Plateau may be partly caused by local snow cover anomalies. Some previous studies (e.g. Namias, 1985; Leathers and Robinson, 1993) have pointed out that the variability of surface temperature can be regulated, to some extent, by the change in snow cover. Figure 7 shows the anomalies of accumulated snow depth (ASD) for the early and late BOBSM onset categories. Because the Tibetan Plateau snow cover begins to develop in mid-September and progresses very quickly after mid-October or early November, the ASD from November (of the previous year) to March can be used to represent snow mass variation for each year (Li, 1993; Wu and Qian, 2003). At most stations over the Tibetan Plateau, ASD anomalies are negative in the early onset category (Fig. 7a), corresponding to positive temperature (600 hPa) and thickness (200–500 hPa) anomalies (Fig. 5). In contrast, most stations exhibit positive anomalies in the late onset category (Fig. 7b). These indicate that an early (late) BOBSM onset is associated with less (more) Tibetan Plateau snow accumulation during the preceding winter.

## 5. Conclusions and discussions

Following Mao et al. (2004), we examine the climatological characteristics associated with the summer monsoon onset over the eastern Bay of Bengal (BOB) by considering the variation of the westerly-easterly boundary surface (WEB). During the transitional season, the WEB tilts from southward to northward, suggesting a replacement between the winter and the summer monsoon. The switch of the WEB tilt firstly occurs between 90 and 100°E during the first pentad of May and coincides with the 850 hPa ridgeline splitting and heavy rainfall commencing over the eastern BOB, indicating the onset of the BOB summer monsoon. The climatological onset date determined by the upper tropospheric (200–500 hPa) MTG is similar to those defined by zonal wind at 850 hPa, CMAP precipitation, and OLR. Therefore, the area-averaged MTG (200–500 hPa) near the WEB is used to define the BOBSM onset. Our study shows that the reversal of the MTG can capture the essential features of the BOBSM onset.

The interannual variability of the BOBSM onset is investigated based on the time series of onset dates derived from the MTG. The long-term mean onset date is 2 May, with a standard deviation of 10.1 days. Composite results show that early (late) BOBSM onset follows excessive (deficient) rainfall over the western Pacific and anomalous lower tropospheric cyclonic (anticyclonic) circulation in the northern Indian Ocean – western Pacific region, coincident with strong (weak) equatorial westerly anomalies in the preceding winter and spring. Changes of atmospheric temperature and thickness are

observed to be dynamically consistent with those in the upper tropospheric wind field. Prior to an early (late) BOBSM onset, significantly positive (negative) thickness anomalies appear over the Tibetan Plateau and migrate westward, accompanied by an anomalous upper tropospheric anticyclonic (cyclonic) circulation. These strong signals suggest that the Tibetan Plateau has an important impact on middle and upper tropospheric temperature anomalies, leading to a change in the land–sea thermal contrast.

The interannual variations of the BOBSM onset date are significantly correlated with the SST anomalies during the preceding winter and spring, suggesting a remote impact of the El Niño (La Niña) event on BOBSM onset. An El Niño (La Niña) event is followed by late (early) BOBSM onset. The changes of the Walker circulation and the local Hadley circulation forced by ENSO may be one of the mechanisms responsible for regulating early/late BOBSM onset. The SST anomalies in the Indian Ocean and western Pacific may cause a change in the land–sea thermal contrast over the Asian sector. On the other hand, the heat source in the equatorial eastern Pacific can warm the entire tropical tropospheric atmosphere, and thus, can also affect the land–sea thermal contrast. Our study suggests that the precursor signals around the Tibetan Plateau are partly caused by local snow cover anomalies. An early (late) BOBSM onset is usually preceded by less (more) snow accumulation over the Tibetan Plateau during the preceding winter.

It is well known that the summer monsoon circulation can be explained by diabatic forcing due to condensation heating, sensible heating, and radiation cooling (e.g. Rodwell and Hoskins, 1996; Ose, 1998). On the one hand, the diabatic heating contributes as an external forcing to the increase of local temperature based on the thermodynamic equation. On the other hand, the monsoon circulation responds to differential heating between the regions of cooling and heating. These features thus indicate that there exists a nonlinear feedback between heating and monsoon circulation dynamics. Krishnamurti (1985) suggested that the Indian monsoon can largely be viewed as a response of the circulation to differential heating, and the mode of migration of the heating region from northern Burma in May to the foothills of the Himalayas (eastern Tibet) in June is a critical factor in determining the onset of the Indian Monsoon. These imply that the temporal and spatial variation of the heat source should play some role in the seasonal transition associated with the BOBSM onset. However, there are no directly observed heating data available. The NCEP-NCAR heating fluxes as model output products are six-hour averages starting at the reference time, thus the heating distribution, as derived from these flux data, can only help us quantitatively understand the role of differential heat in the BOBSM onset. The distributions of diabatic heating anomalies can be roughly found from Fig. 3, because released latent heating is the dominant component that composes the total diabatic heating, especially over ocean areas. As suggested by Krishnamurti and Ramanathan (1982), such a west-east heating difference between Indian Ocean and western Pacific is favorable for an acceleration of low-level divergent westerly winds, further enhancing the rotational winds over the BOB, via energetic transform among the rotational, divergent and available potential energies.

Wu and Zhang (1998) emphasized the importance of sensible heating over the Tibetan Plateau in the increase of air column temperature. Climatologically, sensible heating flux greater than $50\,\mathrm{W\,m^{-2}}$ occurs over the entire Tibetan Plateau in April to May. Such diabatic heating flux can warm the middle and upper tropospheric atmosphere. In this sense, sensible heating flux anomalies may partly contribute to positive thickness anomalies around the plateau, because horizontal and vertical temperature advections are also responsible for the increase of air column. Based on snow depth anomalies shown in Fig. 7, it may be inferred that the sensible heating flux anomalies, to a certain extent, influence the BOBSM onset. Of course, zonal and meridional variations of the differential heating may lead co-operatively to an abnormal BOBSM onset.

**Acknowledgments**

The NCEP/NCAR reanalysis data are provided by the NOAA-CIRES Climate Diagnostics Center, Boulder, Colorado, USA, from their web site at http://www.cdc.noaa.gov/. This research was supported by National Basic Research program of China (Grant No.2005CB422004) and Natural Science Foundation of China under Grants 40375022, 40523001, 40325015, and 40475027.

## References


Ananthakkrishnan R, Soman MK (1988) The onset of the south-west monsoon over Kerala: 1901–1980. J Climatol 8: 283–296

Barnett TP, Dumenil L, Schlese U, Roceckner E, Latif M (1989) The effect of Eurasian snow cover on regional and global climate variations. J Atmos Sci 46: 661–685

Chan JCL, Wang Y, Xu J (2000) Dynamic and thermodynamic characteristics associated with the onset of the 1998 South China Sea summer monsoon. J Meteor Soc Japan 78: 367–380

Chen TC, Chen JM (1993) The 10–20-day mode of the 1979 Indian monsoon: Its relation with the time variation of monsoon rainfall. Mon Wea Rev 121: 2465–2482

Dey B, Kathuria SN (1986) Himalayan snow cover area and onset of summer monsoon over Kerla, India. Mausam 37: 193–196

Ding Y, Liu Y (2001) Onset and the evolution of the summer monsoon over the South China Sea during SCSMEX field experiment in 1998. J Meteor Soc Japan 79: 255–276

Flohn H (1957) Large-scale aspects of the ''summer monsoon'' in South and East Asia. J Meteor Soc Japan (75th Ann Vol): 180–186

Gill AE (1980) Some simple solutions for heat-induced tropical circulation. Quart J Roy Meteor Soc 106: 447–462

Hahn DG, Shukla J (1976) An apparent relationship between Eurasian snow cover and Indian monsoon rainfall. J Atmos Sci 33: 2461–2462

Joseph PV, Eischeid JK, Pyle RJ (1994) Interannual variability of the onset of the Indian summer monsoon and its association with atmospheric features, El Niño, and sea surface temperature anomalies. J Climate 7: 81–105

Ju J, Slingo JM (1995) The Asian summer monsoon and ENSO. Quart J Roy Meteor Soc 121: 1133–1162

Kalnay E, et al (1996) The NCEP/NCAR 40-year reanalysis project. Bull Amer Meteor Soc 77: 437–471

Kawamura R (1998) A possible mechanism of the Asian summer monsoon – ENSO coupling. J Meteor Soc Japan 76: 1009–1027

Krishnamurti TN (1985) Summer monsoon experiment – A review. Mon Wea Rev 113: 344–363

Krishnamurti TN, Ramanathan Y (1982) Sensitivity of the monsoon onset to differential heating. J Atmos Sci 39: 1290–1306

Krishnamurti TN, Ardanuy P, Ramanathan Y, Pasch R (1981) On the onset vortex of the summer monsoons. Mon Wea Rev 109: 344–363

Lau KM, Yang S (1997) Climatology and interannual variability of the Southeast Asian summer monsoon. Adv Atmos Sci 14: 141–162

Leathers DJ, Robinson DA (1993) The association between extremes in North American snow cover extent and United States temperatures. J Climate 6: 1345–1355

Li C, Yanai M (1996) The onset and interannual variability of the Asian summer monsoon in relation to land–sea thermal contrast. J Climate 9: 358–375

Li J, Chou J (1998) Dynamical analysis on splitting of subtropical high-pressure zone – Geostrophic effect. Chinese Sci Bull 43: 1285–1288

Li PJ (1993) Characteristics of snow cover in western China. Acta Geograph Sin 48: 505–514

LinHo, Wang B (2002) The time-space structure of Asian summer monsoon-A fast annual cycle view. J Climate 15: 2001–2019

Mao J, Chan JCL, Wu G (2004) Relationship between the onset of the South China Sea summer monsoon and the structure of the Asian subtropical anticyclone. J Meteor Soc Japan 82: 845–859

Meehl GA (1987) The annual cycle and interannual variability in the tropical Pacific and Indian Ocean regions. Mon Wea Rev 115: 27–50

Miyakoda K, Kinter III JL, Yang S (2003) The role of ENSO in the South Asian monsoon and pre-monsoon signals over the Tibetan Plateau. J Meteor Soc Japan 81: 1015–1039

Namias J (1985) Some empirical evidence for the influence of snow cover on temperature and precipitation. Mon Wea Rev 113: 1542–1553

Namias J, Yuan X, Cayan DR (1988) Persistence of North Pacific sea surface temperature and atmospheric flow patterns. J Climate 1: 682–703

Ose T (1998) Seasonal change of Asian summer monsoon circulation and its heat source. J Meteor Soc Japan 76: 1045–1063

Rodwell MJ, Hoskins BJ (1996) Monsoons and the dynamics of deserts. Quart J Roy Meteor Soc 122: 1385–1404

Sewell RD, Landman WA (2001) Indo-Pacific relationships in terms of sea-surface temperature variations. Int J Climatol 21: 1515–1528

Soman MK, Slingo JM (1997) Sensitivity of the Asian summer monsoon to aspects of sea surface temperature anomalies in the tropical Pacific Ocean. Quart J Roy Meteor Soc 123: 309–336

Tanaka M (1992) Intraseasonal oscillation and the onset and retreat dates of the summer monsoon over the east, southeast and western north Pacific region using GMS high cloud amount data. J Meteor Soc Japan 70: 613–629

Tao S, Chen L (1987) A review of recent research on the East Asian summer monsoon in China. In: Chang CP, Krishnamurti TN (eds) Monsoon meteorology. Oxford University Press, pp 60–92

Ting M, Held IM (1990) The stationary wave response to a tropical SST anomaly in an idealized GCM. J Atmos Sci 47: 2546–2566

Trenberth KE (1990) Recent observed interdecadal climate changes in the Northern Hemisphere. Bull Amer Meteor Soc 71: 988–993

Ueda H, Yasunari T (1998) Role of warming over the Tibetan Plateau in early onset of the summer monsoon over the Bay of Bengal and South China Sea. J Meteor Soc Japan 76: 1–12

Walsh JE, Jasperson WH, Ross B (1985) Influences of snow cover and soil moisture on monthly air temperature. Mon Wea Rev 113: 756–768

Wang B, LinHo (2002) Rainy season of the Asian–Pacific summer monsoon. J Climate 15: 386–398

Webster PJ, Yang S (1992) Monsoon and ENSO: Selectively interactive systems. Quart J Roy Meteor Soc 118: 877–926

Webster PJ, Magana VO, Palmer TN, Shukla J, Tomas RA, Yanai M, Yasunari T (1998) Monsoons: processes, pre-

dictability, and prospects for prediction. J Geophys Res 103: 14451–14510

Wu G, Zhang Y (1998) Tibetan Plateau forcing and the monsoon onset over South Asia and the South China Sea. Mon Wea Rev 126: 913–927

Wu T, Qian Z (2003) The relation between the Tibetan winter snow and the Asian summer monsoon and rainfall: an observational investigation. J Climate 16: 2038–2051

Wu ZX, Newell RE (1998) Influence of sea surface temperatures on air temperatures in the tropics. Clim Dyn 14: 275–290

Xie A, Chung YS, Liu X, Ye Q (1998) The interannual variations of the summer monsoon onset over the South China Sea. Theor Appl Climatol 59: 201–213

Xie P, Arkin PA (1997) Global precipitation: A 17-year monthly analysis based on gauge observations, satellite estimates and numerical model outputs. Bull Amer Meteor Soc 78: 2539–2558

Xu J, Chan JCL (2001) First transition of the Asian summer monsoon in 1998 and the effect of the Tibet-tropical ocean thermal contrast. J Meteor Soc Japan 79: 241–253

Yanai M, Li C, Song Z (1992) Seasonal heating of the Tibetan Plateau and its effects on the evolution of the Asian summer monsoon. J Meteor Soc Japan 70: 319–351

Yang S, Lau KM (1996) Precursory signals associated with the interannual variability of the Asian summer monsoon. J Climate 9: 949–964

Yasunari T, Kitoh A, Tokioka T (1991) Local and remote responses to excessive snow mass over Eursasia appearing in the northern spring and summer climate – A study with the MRI-GCM. J Meteor Soc Japan 69: 473–487

Zhang Y, Li T, Wang B, Wu G (2002) Onset of the summer monsoon over the Indochina Peninsula: Climatology and interannual variations. J Climate 15: 3206–3221

Authors' address: Dr. Jiangyu Mao (e-mail: mjy@lasg.iap.ac.cn), Guoxiong Wu, State Key Laboratory of Numerical Modeling for Atmospheric Sciences and Geophysical Fluid Dynamics (LASG), Institute of Atmospheric Physics, Chinese Academy of Sciences, P.O. Box 9804, Beijing 100029, China.